

1
2
3
4
5
6
7
8
9
10
11
12
13
14
15
16
17
18
19
20
21
22

DR JENNA MARGARET CROWE-RIDDELL (Orcid ID : 0000-0003-2794-2914)

Article type : Original Research

A guide for optimal iodine staining and high-throughput diceCT scanning in snakes

Sean Callahan^{1,4*} and Jenna M. Crowe-Riddell^{1,2*}, Ramon S. Nagesan¹, Jaimi A. Gray³, Alison R. Davis Rabosky^{1,2}

* Co-first authors, these authors contributed equally to the research in this manuscript

¹ Museum of Zoology, University of Michigan, Ann Arbor MI, 48108, USA

² Ecology and Evolutionary Biology, University of Michigan, Ann Arbor MI 48109, USA

³ Florida Museum of Natural History, University of Florida, Gainesville, FL 32611

⁴ Department of Biology, Eastern Michigan University, Ypsilanti, MI, 48197, USA

Corresponding author: jmcr@umich.edu

Running head: Guide to diceCT scanning snakes

Manuscript for consideration in *Ecology and Evolution*.

Word count: 6,975

This is the author manuscript accepted for publication and has undergone full peer review but has not been through the copyediting, typesetting, pagination and proofreading process, which may lead to differences between this version and the [Version of Record](#). Please cite this article as [doi: 10.1002/ECE3.7467](https://doi.org/10.1002/ECE3.7467)

This article is protected by copyright. All rights reserved

23

24 Abstract

25 Diffusible iodine-based contrast-enhanced Computed-Tomography (diceCT) visualizes soft-tissue from
26 microCT (μ CT) scans of specimens to uncover internal features and natural history information without
27 incurring physical damage via dissection. Unlike hard-tissue imaging, taxonomic sampling within diceCT
28 datasets are currently limited. To initiate best practices for diceCT in a non-model group, we outline a
29 guide for staining and high-throughput μ CT scanning in snakes. We scanned the entire body and one
30 region of interest (i.e., head) for 23 specimens representing 23 species from the clades Aniliidae,
31 Dipsadinae, Colubrinae, Elapidae, Lamprophiidae and Viperidae. We generated 82 scans that include
32 1.25% Lugol's iodine stained (soft tissue) and unstained (skeletal) data for each specimen. We found
33 that duration of optimal staining time increased linearly with body size; head radius was the best
34 indicator. Post-reconstruction of scans, optimal staining was evident by evenly distributed grayscale
35 values and clear differentiation among soft-tissue anatomy. Under and over stained specimens
36 produced poor contrast among soft-tissues, which was often exacerbated by user bias during "digital
37 dissections" (i.e., segmentation). Regardless, all scans produced usable data from which we assessed a
38 range of downstream analytical applications within ecology and evolution (e.g., predator-prey
39 interactions, life history, and morphological evolution). Ethanol de-staining reversed the known effects
40 of iodine on the exterior appearance of physical specimens, but required substantially more time than
41 reported for other de-staining methods. We discuss the feasibility of implementing diceCT techniques
42 for a new user, including approximate financial and temporal commitments, required facilities, and
43 potential effects of staining on specimens. We present the first high-throughput workflow for full-body
44 skeletal and diceCT scanning in snakes, which can be generalized to any elongate vertebrates, and
45 increases publicly available diceCT scans for reptiles by an order of magnitude.

46 **Keywords:** anatomy, computed-tomography, education, herpetology, imaging, morphology, museum
47 collections, Peruvian Amazon

48 1. Introduction

49 Museum collections are foundational to studies in ecology and evolutionary biology because
50 they create a permanent record of how organisms respond to changing environmental, climatic and
51 ecological forces (Lister et al., 2011). Access to collections was historically limited to those with the
52 means to visit a museum in person. The recent revolution to digitize museum data has begun

53 “unlocking” these collections and democratizing data on a global scale (Hedrick et al., 2020). These
54 digitization initiatives produce great innovation in both education and research (Bakker et al., 2020),
55 with new applications across biology, especially morphology through non-destructive specimen imaging
56 (Gray, Sherratt, Hutchinson, & Jones, 2019; Paluh, Stanley, & Blackburn, 2020). However, the most
57 commonly used imaging technology (microcomputed tomography, or μ CT) only detect mineralized
58 features (e.g., bones, teeth) with limited capacity for visualizing soft-tissue anatomy, which are vital data
59 for understanding integrated organismal systems.

60 Diffusible iodine-based contrast-enhanced μ CT (diceCT) enhances contrast of soft-tissues by
61 submerging or injecting preserved specimens with an iodine solution prior to scanning (Metscher, 2009;
62 Gignac & Kley, 2014; Gignac et al., 2016). Post-scanning, the iodine solution can be removed via leaching
63 or chemical de-staining, which has led to diceCT gaining popularity as a non- to minimally-destructive
64 technique (see Hedrick et al., 2018; Early et al., 2020). In addition to digital imaging of soft-tissues in
65 three dimensions (3D), diceCT can also provide access to ecological data or “natural history bycatch”
66 that includes diet records of both hard- and soft-bodied prey, parasite loads, and clutch sizes or stages
67 of reproductive development. The combination of traditional μ CT and emerging diceCT techniques can
68 create integrative datasets for museum specimens (e.g. Clement et al., 2015; Fabbri et al. 2017), which
69 can be shared widely and used to address questions of both form and function in biology.

70 DiceCT has great potential to propel comparative morphological studies forward (Gignac & Kley,
71 2018), but the systematic collection of diceCT data is currently limited in this field. Taxonomic
72 representation among vertebrates is lacking; data are biased towards mammals with a narrow
73 representation of non-model organisms within reptiles, amphibians and birds (Gignac et al., 2016,
74 references therein). A lack of taxon-specific protocols, as well as an underreporting of diceCT
75 successes/failures are likely hindering progress in diceCT techniques (Gignac et al., 2016). To increase
76 available diceCT datasets, we need a guide to initiate best practices for streamlined data generation and
77 curation that is tailored to specific taxonomic groups as has been done for traditional μ CT methods (e.g.,
78 see “scan all fishes,” Buser et al., 2020).

79 Snakes are an ecologically diverse clade of limbless squamate reptiles with ~3879 species
80 currently recognized from 20 families (Uetz, 2020). Snakes have the largest range of body sizes in any
81 tetrapod clade besides mammals, with adult ranging from 10 cm to 9 m in length depending on the
82 species. Snakes have been foundational to research on extreme phenotypes, especially their
83 morphological and ecological adaptations for prey capture, physiology, locomotion, and sensory

84 specializations (Lillywhite, 2014). Recent non-destructive imaging in snakes include studies in
85 locomotion (Capano, 2020), skull and fang morphology (Da Silva et al., 2018; du Plessis, Broeckhoven, &
86 le Roux, 2018), neural and sensory systems (Gignac & Kley, 2018; Macri, Savriama, Khan, & Di-Poï, 2019),
87 and previously unknown cephalic vasculature (Palci et al., 2019). DiceCT datasets (head only) have been
88 published for just three snakes: an annulated sea snake (*Hydrophis cyanocinctus*), a western
89 diamondback rattlesnake (*Crotalus atrox*) and a European viper (*Vipera berus*) (Gignac et al., 2016; Palci
90 et al., 2019). Together, these studies can enhance our understanding of the ecology and evolution of
91 transitions to elongate forms, as well as the broad diversification processes that follow these transitions.

92 In this study, we diceCT scanned 23 species of snakes with the following goals: (i) Determine the
93 optimal packing and iodine staining procedure to visualize soft-tissues in a taxonomically diverse set of
94 snakes encompassing a range of body and head sizes, (ii) devise an efficient workflow for high-volume
95 scanning of specimens that is optimized for longevity of digital specimens with minimal damage to
96 physical specimens, and (iii) assess the range of downstream applications made possible by making
97 these data available to the scientific community. We contextualize this workflow in relation to project
98 timelines, data sharing and future high-throughput diceCT studies in snakes and other underrepresented
99 taxa, especially their potential use across diverse research and educational initiatives.

100 2. Materials and Methods

101 2.1 Specimen selection and preservation

102 We stained and scanned a single specimen each from 23 species (n = 23 individuals) in the snake
103 clades Aniliidae, Dipsadinae, Colubrinae, Elapidae, Lamprophiidae and Viperidae (following
104 nomenclature in Pyron, Burbrink, & Wiens, 2013; Table 1). Specimens encompassed a range of body
105 sizes: snout to vent length (SVL) between 104 mm and 1840 mm, and body mass between 8.4 g to and
106 1250 g. Specimens were sourced from the University of Michigan Museum of Zoology (UMMZ) and
107 Museo de Historia Natural de la Universidad Nacional Mayor de San Marcos (MUSM). They had been
108 previously fixed in 10% formalin, preserved in 75% ethanol (EtOH) and stored at UMMZ, Ann Arbor,
109 Michigan, USA. The majority of specimens were collected during trips to Peru and Nicaragua from 2016
110 to 2019, and euthanized and fixed 24 h after capture. All field collection protocols were approved by the
111 University of Michigan Institutional Animal Care and Use Committee (#PRO00006234, #PRO00008306)
112 and collections made through permits from the Servicio Nacional Forestal y de Fauna Silvestre (029-
113 2016-SERFOR-DGGSPFFS, 405-2016-SERFOR-DGGSPFFS, 116-2017-SERFOR-DGGSPFFS) and Ministerio

114 del Ambiente y los Recursos Naturales de la República de Nicaragua (DGB-IC-058-2017, DGPNB-IC-019-
115 2018, DGPNB-IC-020-2018, DGPNB-IC-002-2019).

116 2.2 Workflow for staining and micro-CT scanning

117 2.2.1 Scheduling scans

118 For 18 specimens, we conducted two unstained and two stained scans per specimen: (i) skeletal
119 scan of the entire specimen prior to staining, (ii) skull scan of the head as a region of interest (ROI), (iii)
120 diceCT scan of the entire specimen, and (iv) diceCT scan of the head ROI. The remaining five specimens
121 were scanned only twice: a skeletal (i) and diceCT (iii) scan of the entire specimen for *Pseustes*
122 *sulphureus*, and a skull ROI (ii) and diceCT ROI (iv) each for *Leptophis ahaetulla*, *Xenopholis scalaris*,
123 *Micrurus lemniscatus* and *Micrurus obscurus* (see Table 1). These specimens were stained and scanned
124 early in the development of our methodology and were included in the study because they demonstrate
125 inadequate packing/staining and/or broaden the range of body sizes.

126 Scan times were ~14 min for each skeletal scan and ~3.75 h for diceCT at their respective
127 standard parameters (Supplementary Table S1). Entire body and ROI diceCT scans were performed
128 sequentially overnight using a batch scan program. Given the significantly longer scan time of diceCT
129 compared to skeletal scans, scanning at night maximized workflow efficiency and data generation during
130 the day, and allowed the specimen to settle in the packing media. Overnight batch scanning was
131 paramount to ensuring a high-throughput workflow pace; it also allotted extra time for any unexpected
132 delays and setbacks we experienced

133 2.2.2 Iodine staining

134 Once skeletal scans were complete, we stained all specimens by submersion in 1.25% (total
135 solute) Lugol's iodine solution ($I_2 + KI + H_2O$) in the dark, following Gignac et al. (2014). Preparation
136 protocols for reagents and solutions are provided in Appendix 1. We prepared approximately 3.85 L of
137 Lugol's iodine solution at a time. To ensure specimen quality and longevity, we only stained preserved
138 specimens once, although it is unknown what consequences, if any, arise from multiple bouts of
139 staining. Given that optimal staining duration varied per specimen, we planned diceCT scans at least 1-2
140 weeks in advance.

141 Specimens were downgraded in stepwise concentrations of EtOH (75%, 50%, 25%); spending 2-4
142 days at each concentration (Figure 1, Step 1). The EtOH downgrade may lessen the effects of osmotic

143 shock of moving specimens from alcohol to the water-based Lugol's iodine solution, and vice versa
144 (pers. obs. S. Callahan, GE Schneider; Simmons, 2014). Specimens were then immersed in large
145 containers of 1.25% Lugol's iodine (Figure 1, Step 2). To assess whether the 1.25% Lugol's iodine had
146 completely perfused the submerged specimen, we examined the opacity of the solution every 24 h
147 (Figure 1, Step 3). Complete tissue saturation was indicated, in part, when the solution was opaque for
148 at least 72 h (Figure 2). If the solution changed from opaque to translucent, this indicated incomplete
149 diffusion and the solution was replaced with fresh 1.25% Lugol's iodine and again monitored for
150 saturation. The skin of adequately stained specimens was dark amber in colour, which often obscured
151 any external colour patterns on the specimen that were visible prior to staining (see Figure 2 for ideal
152 staining). Specimens with incomplete diffusion typically looked 'under-stained', i.e., skin was a light red
153 or yellow in external appearance.

154 If optimal staining duration could not be determined by inspecting solution opacity and/or
155 external appearance of specimens, we performed a quality assessment scan to assess the staining
156 progress (Figure 3). A brief scan was conducted at the standard diceCT parameters (see Table S1) and
157 aborted a few minutes after the scan began, as we only needed a few tomographic slices to assess soft
158 tissue contrast. If the specimen was under-stained, there was a visible diffusion gradient (Figure 3). If
159 the specimens was overstained, there was very minimal contrast among the internal soft tissues.

160 We also tested for the potential effects of specimen size on staining duration. We took standard
161 measurements of specimen size (SVL, mass, and head diameter) for 20 specimens preserved recently (1-
162 3 years old), and three historical specimens (25 – 95 years old) already present in the UMMZ collections
163 (Table 1). Effects of specimen mass were only tested for individuals that were weighed prior to
164 preservation (n = 20) to minimize measurement error due to preservation fluid. We calculated diffusion
165 rate by dividing the radius (mm) of the head by total staining duration (d).

166 2.2.3 Packing

167 Any movement during scanning will create a misalignment of the center of rotation, yielding
168 poor or unusable data (e.g., blurred edges within two dimensional [2D] tomography slices). To ensure
169 high-quality data, specimens should be packed to adequately restrict specimens to prevent movement
170 during scanning.

171 Snake specimens are typically fixed in a tightly-coiled spiral during the preservation process to
172 accommodate their elongate, limbless bodies in the specimen jars. This presents unique challenges for

173 packing snakes for CT-scanning. Limbed vertebrate specimens are typically preserved in a manner that
174 separates the limbs from the rest of the body, and they can be prepared for scanning by packing them
175 into a flat and rectangular bag, without excessive manipulation of the specimen itself. In turn, head ROI
176 scans of limbed vertebrates are relatively simple to conduct without interference from other anatomical
177 structures. The coiled position of preserved snakes is adequate, although not ideal, for full body scans,
178 but it becomes problematic for head ROI scans because the head is not spatially separated from the
179 body coils. As a result, the x-rays will attenuate as they are absorbed through or deflected off non-ROI
180 parts of the body. This problem is more pronounced for ROI scans because the head is often nested
181 between large body coils, and the resulting scans of the head ROI are reduced in quality. Additionally,
182 coiling the specimen upon itself leaves a considerable amount of air trapped in the packing bag, which
183 increases the potential for desiccation.

184 To address these challenges, we prepared coiled specimens for scanning by using customized
185 plastic bags that had been cut and heat-sealed. We cut poly tubing plastic (Uline, WI, USA) to 5-10 cm
186 longer than the total length of each snake and sealed lengthwise, leaving the ends unsealed (i.e., open)
187 (Figure 1b). We also placed a piece of string, twice the length of the plastic bag, inside the bag with
188 excess string coming out of the open ends. One end of the string was tied around the specimen's neck,
189 then the specimen was pulled through the bag by pulling the loose string on the other end. The string
190 was removed and the anterior-end of the bag was heat sealed, leaving some extra space at both ends of
191 the specimen. Any metal tags were replaced with paper tags until after de-staining was complete.

192 To keep specimens in place during scanning, we packed them into appropriately sized
193 containers. The container should be large enough to manipulate the specimen easily and tightly pack the
194 specimen with minimal packing media. We typically chose wide mouthed, round containers (5-15 cm
195 diameter; Uline, WI, USA). We found "anti-static packing peanuts" (30% recycled polystyrene, Uline, WI,
196 USA) to be the ideal packing media because the X-rays fully penetrated the packing peanuts and
197 produced minimal noise when rendering the data (especially compared to larger foam sheets, see Figure
198 3a). They are also easy to source, reusable and inexpensive. We tightly filled the empty spaces around
199 the positioned specimen with peanuts to hold the specimen in place during the scan.

200 We positioned specimens in an ascending spiral with the neck and head separated by strategic
201 layers of packing media, with the head in the middle of the container pointing upwards (Figure 1d).
202 Once the container lid was sealed and given a specimen tracker tag (Figure 1, Step 2), the specimen was
203 left to settle to minimize the risk of it movement during scanning. Specimens were left for a minimum of

204 30 min for skeletal scans and 2 h for diceCT scans. We performed full body and head ROI scans
205 sequentially to prevent the need for repacking of specimens between scans.

206 *2.2.4 Mounting*

207 After the specimen had settled in its packing container, we placed it on top of a similarly sized or
208 larger mounting container (Figure 1, Step 3). Mounting containers are empty containers that create
209 spatial separation between the metal platform and the specimen. We placed the stacked containers in
210 the middle of the scanner platform and manipulated using the zoom and y-direction platform joysticks
211 and/or by manually moving the stacked containers. Platform manipulation in the x-direction on the
212 scanner was locked in all scans. We manually repositioned the stacked containers at various degrees of
213 rotation to ensure the ROI always remained visible to the detector panel.

214 *2.2.5 Scanning parameters*

215 We conducted all scans on a Nikon Metrology XTH 225ST μ -CT scanner (Xteck, Tring, UK). We
216 conducted skeletal scans at 85 kilovolts (kV, voltage), 200 micro-amperes (uA, amperage), 250
217 millisecond exposures (ms), 1601 projections, with 2x-frame averaging. We conducted diceCT scans at
218 85kV, 200uA, 250 ms, 3141 projections, with 16x-frame averaging (Table S1). Scans where the voxel size
219 was less than the power were conducted at 120uA. We reconstructed raw tomography projections using
220 CT-3D Pro (Nikon Metrology, Tring, UK), which generated approximately 2000 cross-sectional tagged
221 image file format (TIFF) per data set. For visualisation, we imported the reconstructed images into
222 Volume Graphics (VG) Studio Max version 3.3 (2019, Volume Graphics, Heidelberg, Germany) where
223 they were compiled into 3D renders for segmentation and anatomical analysis.

224 *2.2.6 De-staining*

225 After the diceCT scanning was completed, we de-stained specimens with a series of EtOH
226 solutions (25%, 50%, 75%), leaving the specimen in each EtOH concentration for 2-3 months (Figure 1,
227 Step 5). We periodically replaced the EtOH solution when it reached near complete iodine saturation, as
228 indicated by the dark amber colour of the liquid.

229 2.3 Post-scanning data management and analysis

230 *2.3.1 Data storage and access*

231 All scans produced from this study are available on Morphosource (see Table S2). Once scans were
232 complete, the tomographic projections (.tiffs) were reconstructed into a dataset comprising a cross-
233 sectional image slice stack (each image is a single orthogonal slice through the specimen). Each cross-
234 sectional image slice stack was exported as a 16-bit tiff stack. In addition to the image stack, a Volume
235 Graphics project file (.VGL) was created. This project file facilitates the opening and viewing of the data
236 in Volume Graphics 3.2. The final dataset for each specimen included: raw tomographic projects (.tiffs),
237 cross-sectional image stack (.tiffs), and a Volume graphics project (.VGL). The dataset for each specimen
238 was then backed up onto a pair of 5TB external hard drive (one primary, and one backup).

239 *2.3.2 Digital segmentation of hard and soft tissues*

240 We conducted segmentation in VG Studio Max v3.2, aided by the use of a Wacom Cintiq 22HD
241 tablet version 6.37-3 (Wacom Co., Ltd., Kazo, Saitama, Japan). We used a combination of the “draw” and
242 “region-growing” tools to segment bone from skeletal scans and soft tissue anatomy from diceCT scans.
243 We identified the range of grayscale values (GV) of the anatomical structure of interest using the
244 “navigation cursor” tool, which were used to constrain the selection made by the draw tool. For the
245 region growing tool, a single pixel or cluster of pixels was selected by the user and a grey value threshold
246 set as the +/- range of pixels that will be included in the selection. This pixel range varied among
247 specimens but the typical threshold value was +/- 1000 within the grey values of the anatomical
248 structure of interest.

249 **3 Results**

250 We stained and scanned a total of 23 specimens in 31 weeks (Table 1), generating 41 skeletal
251 scans and 41 diceCT scans (82 scans in total) with 18 specimens consisting of both full body and ROI
252 head scans (mean = 2, range = 0-2 per week). DiceCT scans of the head ROI had higher resolutions
253 (range 0.01001 - 0.02923 voxels) than the full body diceCT (range 0.05116-0.08475 voxels) due to
254 constraints in packing coiled specimens and sequential scan setups (Table S1). Nevertheless, both head
255 and full body diceCT scans yielded good quality data for the variety of downstream applications we
256 detail below.

257 Optimally stained specimens resulted in 2D tomography slices with consistent contrast among
258 all tissues. Under stained specimens generated scans with a narrow GV range, overstained specimens
259 corresponded to broad GV range with overall low voxel counts across values, and optimally stained
260 specimens had a relatively narrower GV range but consistently higher voxel counts across those values

261 (Figure 4). GV is a way of visualizing x-ray attenuation (i.e. a localized reduction in x-ray intensity). On a
262 GV histogram, multiple peaks and a broad range of GV corresponds to optimal contrast, and narrow
263 range (single peaks) tends to correspond to lower contrast. (Figure 4). However, these qualitative
264 assessments of optimal contrast were based on subjectivity of the user viewing the scan and may
265 change depending on which soft-tissue structures the user is most interested in. The most common
266 effect of prolonged staining was an uneven uptake of the iodine solution for some tissues over others,
267 yielding a narrow GV range with overall values that near, match, or exceed the GV limits of the UMMZ
268 Nikon XTH 225S μ -CT scanner. Optimal scans and GV ranges were not directly associated with the total
269 staining duration of specimens (Figure 4a), as there is an interaction with body size. To test the potential
270 effects of specimen size on staining duration, a linear regression analysis was performed on natural log-
271 transformed data. We found that the radius of the head was significantly correlated with the number of
272 days specimens were in 1.25% Lugol's iodine (Figure 5a, $F_{1,21} = 47.70$, $p < 0.001$). There was also a
273 weaker correlation between size (both SVL and mass) and the number of days specimens were in 1.25%
274 Lugol's iodine (Figures 5b and 5c, SVL $F_{1,21} = 12.96$, $p < 0.01$; mass $F_{1,18} = 27.44$ $p < 0.001$). There was no
275 correlation between specimen age and number of days specimens were in 1.25% Lugol's iodine ($F_{1,21} =$
276 0.15 , $p = 0.7073$). The mean iodine diffusion rate was 1 mm per day (SD = 0.34 mm).

277 Prior to scanning, the majority of specimens had small, unilateral dissections to remove tissue
278 from one side of the specimen for use in ongoing molecular projects. Iodine uptake at areas of
279 dissection was considerably quicker than low density structures such as the epidermis or stomach,
280 resulting in oversaturation of tissues adjacent to dissection sites (e.g., cephalic glands). On 2D
281 tomographic slices, these overstained structures appeared oversaturated (i.e., very bright and higher
282 GV), which lowered the contrast of surrounding soft-tissues, and subsequently shifted GV ranges across
283 the entire specimen, which resulted in lower contrast even among adequately-stained soft tissues. This
284 effect was especially problematic for visualising small and/or discrete soft-tissue anatomies, such as
285 nerves and unmyelinated encephalic structures, that failed to render (i.e., invisible) or appeared
286 undifferentiated from surrounding structures. Additionally, external tissues with high surface-to-volume
287 ratio (e.g., tongue, epidermis) were often oversaturated in under stained specimens. Deeper internal
288 tissues (e.g., glands, muscle, bones and neural tissue) had little to no iodine uptake in under stained
289 specimens, and they showed limited ultrastructural morphology and tissue differentiation in appearance
290 when viewed in 2D tomography slices (Figure 4b, *Pseustes sulphureus*). Despite the variability in staining
291 quality, we successfully segmented many internal features from most scans, including venom delivery
292 systems (Figure 6-7), neurosensory structures (Figure 8), and diet items and developing eggs (Figure 9).

293 We used an EtOH de-staining protocol without the use of additional solvents (e.g., sodium
294 thiosulfate), which resulted in highly variable de-staining duration depending on specimen size. Smaller
295 specimens (e.g., *Aparallactus capensis*; 104 mm SVL) were adequately de-stained after 2 months; larger
296 specimens (e.g., *Psuetes sulphureus*; 1840 mm SVL) took over a year to fully de-stain. Some specimens
297 initially displayed altered morphological characteristics from the staining process, especially external
298 and internal discoloration of soft tissue and dehydration. The effects of specimen dehydration were
299 particularly visible in the eyes, which presented with concave and wrinkled corneas. However, we found
300 that discolouration and dehydration were fully reversible over time using the EtOH downgrading and
301 upgrading method outlined (Figure 1 Step 1 and 5; Figure 2).

302 4. Discussion

303 We present a protocol to efficiently stain, pack, mount, scan and de-stain museum specimens
304 from a taxonomically diverse range of snakes, applicable to high-throughput data generation for any
305 elongate vertebrate. Our protocol optimises quality of μ CT data and 3D reconstructions, maximizing
306 usability and longevity of “digital specimens” without compromising the integrity of physical museum
307 specimens. There are many benefits of incorporating diceCT scanning into μ CT workflows, as it creates a
308 near-complete digital copy of internal anatomy that can be shared widely with limited destruction to
309 specimens (cf. to traditionally dissection methods). However, challenges for diceCT include a substantial
310 time commitment in the staining and de-staining process, complex analyses of 3D soft-tissue anatomy,
311 and the potential risk of long-term damage to specimens, especially if specimens are stained more than
312 once. Here, we recommend best practices for optimizing μ CT workflows for snakes while mitigating
313 potential risks, and we discuss the potential role for high-throughput generation of diceCT data in
314 research within ecology and evolution.

315 4.1 Packing snakes for μ CT scanning

316 We found that creating form-fitted customized bags provided several advantages for packing
317 coiled snakes. Foremost, this enclosing bag allows for unrestricted positioning of the specimen, which is
318 especially ideal for packing a specimen for ROI scans. The bag also reduces the amount of trapped air,
319 which can dehydrate specimens. Excess iodine solution sometimes collected in the bag, which ultimately
320 caused noise during scanning; vacuum sealing mitigated this issue but increased the potential for skin
321 deformation through contact with the bag. Positioning the snake in a loose ascending spiral, with
322 separation of the head and neck, allowed for minimal attenuation otherwise caused by interference

323 from surrounding structures (Figure 1). The ideal packing position for snakes would be an airtight bag,
324 with the specimen stretched out entirely straight; the scan quality of this specimen could be maximized
325 if scanned helically. However, with the UMMZ scanner, and many types of scanners, helical scanning is
326 currently not an option, and stretching most snakes out their entire length would be too long for the
327 detector panel and or significantly reduce resolution. We recommend that if specimens are being
328 collected for the express purpose of diceCT scanning, then they should be preserved flat with as few
329 spirals as is practical for storage (Figure S1), but note there are new resources for “unwinding”
330 specimens post-scanning (e.g. Williams et al., 2020). These protocols for packing snakes can be applied
331 to other elongate vertebrates including fishes (e.g., hagfish, lampreys, eels), amphibians (caecilians,
332 sirenid and amphiumid salamanders), amphisbaenians, and legless lizards.

333 4.2 Effects of staining on specimens

334 We did not explicitly test how the effects of specimen age, preservation and storage affected
335 the quality of diceCT data. Most specimens used in this study were collected recently (2016-2019),
336 immediately preserved and stored with knowledge that they would ultimately be diceCT scanned. We
337 found that specimen age and duration of preservation were not correlated with total duration of
338 staining, and the three older specimens (collected circa 1950s; Table 1) used in this study did not
339 present any noticeable deviations in staining and or scan quality. Nevertheless, other studies have
340 shown that diceCT of older specimens (e.g., stored in 70% EtOH > 70 years) yield 2D tomography slices
341 with narrow GV ranges and thus poorly differentiated soft-tissue anatomy (Gignac et al., 2016; Hughes
342 et al., 2016). Future studies should aim to test the effect of specimen age as well as how preservation
343 and storage affect quality of diceCT scans.

344 The physical effects of the 1.25% Lugol’s iodine appeared to be fully reversible using an EtOH de-
345 staining protocol. This protocol was selected over other existing de-staining methods in the interest of
346 maintaining specimen quality and longevity. Using a <10% sodium thiosulfate solution for iodine de-
347 staining can dramatically reduce the staining duration and immediately revert specimens to their
348 original colour (Schmidbaur, Keklikoglou, Metscher, & Faulwetter, 2015). However, preliminary evidence
349 suggests that using a sodium thiosulfate solution increases calcium solubility that potentially caused
350 decalcification of ossified structures (Mataic & Bastani, 2006). Thus, we took a cautious approach and
351 chose only EtOH de-staining, which resulted in substantial greater de-staining duration, particularly for
352 large specimens (up to 1 year). The sodium thiosulfate method is used regularly and successfully in other
353 labs with no detectable negative effects, provided that the concentration of sodium thiosulfate is kept

354 very low (<1%), and the specimen remains in sodium thiosulfate for short periods of time (pers obs,
355 J.A.G.). Demineralization has also been observed in avian specimens that were immersed in 1.25-3.75%
356 Lugol's iodine for longer durations, i.e., 5-10 weeks cf. 3-12 days used in the present study (Early et al.,
357 2020). Our staining durations are quicker than those reported in other studies (Gignac et al., 2016),
358 which may be due variations in our protocol (e.g. EtOH downgrade, size of staining vessels), lab set up
359 (e.g. ambient temperature) and/or the high surface to volume ratio of snakes. More studies are needed
360 on a variety of taxa to test the potential effects of staining and de-staining on museum specimens, but
361 we view our approach as conservative but successful for minimizing the known effects of iodine staining
362 to specimens.

363 4.3 Financial and temporal considerations

364 High-throughput diceCT projects require a sizable amount of financial and temporal
365 commitments, in addition to a number of key personnel. Researchers need access to a μ CT scanner for
366 prolonged and uninterrupted scanning, which we mainly performed overnight. These scanning sessions
367 must be planned in advance to ensure that specimens are removed from the staining solution at the
368 appropriate times, which can be challenging because specimens of varying sizes stain at different rates
369 (Figure 5). In addition to reserving μ CT scanners for prolonged times, researchers should anticipate
370 delays for setbacks and maintenance of CT-scanner equipment. During this study, our timeline was
371 frequently altered/extended due to necessary but unscheduled maintenance, timing filament changes,
372 and unexpected program errors, which resulted in the subsequent abortion of batch scan programs.

373 An estimate of financial costs associated with diceCT scanning at the UMMZ is provided in Table
374 2. Based on these estimates, our approximate cost of generating a single diceCT scan of a snake was
375 \$216 (approximately 4.5 h to scan at \$48/h), which we present as an exemplar price point to initiate
376 budget discussions for researchers considering a diceCT project. This estimate is based on hourly
377 operational costs at a facility that is already set up for diceCT scanning (Table 2). However, these costs
378 will vary considerably depending on workstation requirements, type of CT-scanner, how time is billed for
379 shared CT-scanners, and number of technicians/personnel needed for scanning. Costs could be
380 substantially lowered by sharing scanners, software, and training with other research/medical
381 laboratories. A variety of open-access and free-to-use software are available for analysis and
382 segmentation of CT data including Dragonfly, MeshLab, 3D Slicer, FIJI and Blender. Choice of software
383 for rendering and segmenting scans depends on the intersection of many factors including cost,
384 computing power, and available time to users to learn software (for discussion see Buser et al., 2020).

385 Finally, a data management plan is vital to ensure data longevity, access, and dissemination for research
386 and educational initiatives (see Appendix 2 for details of the data management plan used in this study).

387 For data storage, consider the total number and type of scans that will be generated, as each
388 diceCT datasets can be in excess of 20 GB. While external hard drives are easily accessible and allow for
389 data mobility between workstations, they are prone to failure and easily damaged or lost. Data can also
390 be stored on “cloud” based servers, but users must consider subscription costs and international privacy
391 laws of these services. An alternative to cloud- based storage is Redundant Array of Inexpensive Disks
392 (RAID) that can allow multiple workstations to be networked to a central data hub. These options may
393 be more secure and offer redundancy that external hard drives do not, but at increased cost and lower
394 portability.

395 4.4 Challenges and opportunities of digital segmentation

396 One of the primary challenges of analyzing diceCT data is interpreting the overwhelming
397 complexity of soft-tissue anatomy. Upon opening μ CT slice data in a segmenting software, users are
398 inundated with the entirety of internal and external morphology. Successful segmentation is the key
399 step that transforms raw CT scans into usable morphological and life history information, critical to the
400 wide array of downstream research questions and education goals within ecology and evolutionary
401 biology. Identifying and segmenting pertinent anatomical structures is complicated by the overlapping
402 range of GV among internal anatomy, in addition to the already existing anatomical variation (e.g.,
403 shape, size and cell types) and interaction (e.g., networks of blood vessels and nerves). We found that
404 different segmentation tools and approaches were needed depending on the user’s ROI. For example,
405 the brain is a large, lobed structure with varying GV ranges depending on the lobe region, thus relying
406 on a thresholding tool for defining a set GV range is ineffective. Given that the brain is encased in a
407 cranium (in reptiles and birds), it is relatively discrete from other cephalic organs. This feature of neural
408 anatomy allows the user to add “scaffolds” to the CT stack, creating a closely clipped box around the
409 brain and preventing overflow of thresholds values with GV of adjacent tissues. This technique can be
410 used for other discrete structures such as the retina inside the eye. Other anatomical structures can be
411 made discrete under diceCT due to variation in density and therefore GV ranges, e.g. intraocular lens,
412 vomeronasal organs, heat pit membranes, and diet items.

413 A range of approaches and tools can be used for segmenting non-discrete and/or finer-scale and
414 intricately shaped structures or networks of structures, such as nerves or blood vessels (Figure 8; Figure

415 S2). Image enhancements can be performed in various software such as Fiji (Schindelin et al., 2012) and
416 AVIZO (version 2020.1, Thermo Fisher Scientific, MA, USA) to make segmentations easier to complete.
417 Alterations to enhance the boundaries between structures, such as a Gamma correction or “unsharp
418 mask”, can make adjacent organs discrete and thus easier to segment using thresholding tools (see
419 Zuiderveld, 1994). Similarly, identifying how the ROI interfaces with surrounding anatomy (both in the
420 diceCT and skeletal scans) by switching back-and-forth between image enhanced and skeletal scans can
421 help determine the boundaries between structures and orient users while segmenting ROIs. For
422 example, segmentation of the venom delivery system (Figure 6) was aided by referencing traditional
423 dissection of the original specimen and combining the skeletal and diceCT scans to find the connections
424 between fang/maxilla, venom duct and gland. This process was especially important for non-front-
425 fanged species such as colubrids and diploids (Figure 7). Similarly, heat-sensitive membranes and
426 their associated nerves branching from the trigeminal ganglion were revealed in relation to foramina of
427 the maxilla bone from the skeletal scan (Figure S2).

428 A great advantage of diceCT is the creation of digital specimens that allow multiple users to
429 independently characterize and measure the same phenotype across many specimens. However,
430 reproducibility of segmentation in diceCT scans should be tested to ensure repeatability of downstream
431 morphological analyses (e.g., volume and shape measurements). Anecdotally, we found that
432 segmentation variation among users was greatest when (i) poor staining/resolution quality of
433 specimens, and (ii) new users were unfamiliar with segmentation software and/or specimen anatomy.
434 Ensuring that specimens are adequately stained and packed before CT-scanning will ultimately result in
435 easier segmentation for users. To help identify anatomical relationships and increase user familiarity
436 with diceCT, we recommend “exploratory” sessions, whereby the user is exposed to multiple training
437 sets of scans and is free to scroll through adjacent 2D tomography slices. Identifying large, adjacent
438 morphological features or structures can make great ‘reference points’ during segmentation of diceCT
439 scans. Access to taxonomic and anatomical descriptions of specimens are also invaluable reference
440 materials (e.g., Gans 1969-2010, Taub, 1966; Underwood, 1967), and should be used in conjunction with
441 3D models. Despite this extensive literature, however, users experienced difficulty interpreting soft-
442 tissue data because of the complex interconnecting anatomy, overlapping GV ranges, and 3D planes of
443 rotation. Discrepancy in segmentations were highest for the oral and cephalic glands of non-front
444 fanged colubrid snakes (Figure 6-7). Glands from these snakes can vary in size, shape, location, textural
445 appearance, and density (Jackson et al., 2017), as well as being influenced by staining quality. Generally,

446 a combination of approaches (including traditional dissection) may be needed to identify boundaries,
447 interfaces and connections among internal anatomy (Figure 6).

448 4.5 Data curation and storage

449 Data curation is necessary for scientific reproducibility and compliance with institutional
450 regulations (e.g. academic journals, funding bodies). Once scans are hosted online, anyone with an
451 internet connection can access morphological data that was historically inaccessible. There are a
452 number of web- based repositories to store data for this purpose such as Dryad, Morphosource, and
453 DigiMorph. Data may also be archived in research institution libraries (see: UM Libraries Deep Blue
454 Data). Derived μ CT data objects (e.g. segmentations) may fall under the purview of creative commons
455 licenses whereby the original author is credited for their work, but this is not yet an established practice.
456 Finally, data sharing policies for diceCT should be internationally standardised to ensure data are
457 accessible across educational and/or research institutions.

458 We recommend scanning the entire body and ROI of specimens for both traditional μ CT and
459 diceCT, especially for museum collections. This will ensure that specimens are only ever diceCT scanned
460 once, thereby minimizing the potential effects of staining and de-staining process, and providing future
461 access to the entire "digital specimen". Data management plans should implement a standardized
462 system for naming files naming system to facilitate searching large datasets and data archives. Naming
463 conventions should include details of museum and specimens tags, taxonomic identifier, and type of
464 scan (stained or unstained; ROI), and be stored in a hierarchy of directories according to taxonomic rank.
465 Data management plans must ensure that there is sufficient storage capacity for both processing and
466 archiving data. Due to the size of the datasets, 3D rendering, and the complexity of the potential
467 analyses that can be derived from the data, any workstation used will need contain a higher random
468 access memory (RAM) size (64-126GB), a graphics processing unit (GPU) with dedicated memory (2-8
469 GB), and an up to date central processing unit (CPU).

470 4.6 Filaments for CT scanners

471 The lifespan of the filament should be factored into project timelines. The lifespan is dependent
472 on the scanning parameters used, duration of scans, the quality of replacement and alignment, and
473 cleanliness of the CT scanner. At the UMMZ, we use A054X filaments (Agar Scientific, Essex, UK) which
474 typically last about 200 hours of scanning, and AEI style tungsten filaments No.1403 (Ted Pella Inc,
475 California, USA) which were recommended by the Nikon CT scanner manufacturer. However, when our

476 Agar supply was depleted our administrator opted for the Ted Pella Inc. brand, which was at a lower
477 price point (Table 2). As a result, we have noticed a lowered filament lifespan to approximately 125
478 hours. While there is a benefit to saving by ordering equivalent filaments from other vendors, it is best
479 to order the manufacturers recommended parts as it will be more cost effective in the long run.

480

481 4. Recommendations for future diceCT studies

482 DiceCT uncovers internal anatomy of largely inaccessible museum specimens with minimal
483 modification to the original specimen, revolutionizing the capacity for high-throughput phenotyping
484 across the tree of life. DiceCT is a powerful tool to quantify morphological variation, both intra- and
485 inter-specifically, and can be applied to a comparative phylogenetic framework (Figure 8; Macrì et al.,
486 2019). A workflow that ensures both diceCT and skeletal CT scanning ensures a comprehensive digital
487 specimen with access to morphological data and natural history bycatch (Figure 7-9). To ensure that
488 diceCT data can be used in perpetuity and for the broadest range of research and educational
489 applications, the longevity of both the digital and physical specimens should be prioritized. Generating
490 μ CT data is likely to become quicker and easier, resulting in a boom of digital specimens and
491 technological advances to visualize finer-detailed ultrastructure that previously required destructive
492 techniques such as histology. Improvements to post-scanning analysis are also likely to aid users in
493 quickly filtering and segmenting ROIs (see Furat et al., 2019). In this way, diceCT may experience parallel
494 issues to the Big Data generated by DNA sequencing technologies and subsequent lag in expertise to
495 curate and analyze the glut of digital data.

496 DiceCT presents an unprecedented opportunity for analyses of phenotypic evolution and
497 ecological diversification, as well as innovative educational and outreach resources for communicating
498 science to a broader audience. As diceCT technology advances, we should invest in anatomical research
499 that can provide resources of intra- and interspecific variation in anatomy (e.g., 3D visual atlas), as well
500 as comprehensive training of morphologists and investing in open-source software and data
501 repositories.

502

503 **Data availability**

504 The DOIs for diceCT scans of snake heads are available in TableS2, segmentations are available from
505 Morphosource (https://www.morphosource.org/Detail/ProjectDetail/Show/project_id/374) and
506 Sketchfab (<https://sketchfab.com/michiganherpetology>). R script to plot grayscale values and linear
507 regression analyses available on github (<https://github.com/jcrowerriddell/guide-diceCT-snakes>).

508 **Acknowledgements**

509 This work was supported by funding from the University of Michigan to ARDR and the Packard
510 Foundation to Dan Rabosky. Thanks to Greg Pandelis, Erin Westeen, and Greg Schneider for their help in
511 generating a preliminary set of CT scans for this project, as well as the Museo de Historia Natural de la
512 Universidad Nacional Mayor de San Marcos in Peru for specimen loans. We thank Dan Rabosky and Rudi
513 von May for substantial assistance in organising and running the large-scale field expeditions necessary
514 for specimen collection, as well as Conservación Amazónica - ACCA and Project Amazonas for logistical
515 support at Peruvian field stations. We also thank the many additional people who helped collect snakes
516 in the field: Consuelo Alarcón Rodríguez, Arianna Basto, Amaranta Canazas Terán, Heidi Cárdenas,
517 Yohamir Casanca León, Juan Carlos Cusi, Peter Cerda, Mark Cowan, Elar Durand Salazar, Maynor
518 Fernández Mena, Maggie Grundler, Michael Grundler, Valia Herrera, Iris Holmes, Óscar Huacarpuma
519 Aguilar, Edgar Iglesias Antonio, Joanna Larson, Eliz Lennia, César Macahuache Díaz, Jose Martínez
520 Fonseca, Ivan Monagan, Talia Moore, Daniel Nondorf, Greg Pandelis, Imani Russell, Ciara Sánchez
521 Paredes, Roy Santa Cruz Farfán, Briana Sealey, Niery Tafur Olortegui, Tara Smiley, Pascal Title, Erick
522 Vargas Laura, Randi Villarcorta Díaz, and Erin Westeen.

523 **Author contributions**

524 SC, JMC-R, RSN and ARDR conceived the ideas. SC, RSN, JAG and ARDR designed methodology; SC and
525 RSN collected the data; SC, JMC-R and RSN conducted segmentations. SC and JMC-R led the writing of
526 the manuscript. All authors contributed critically to the drafts and gave final approval for publication.

527 **Conflict of Interest**

528 The authors state no conflicts of interest.

529 **References**

530 Bakker, F. T., Antonelli, A., Clarke, J. A., Cook, J. A., Edwards, S. V., Ericson, P. G. P., ... Källersjö, M.
531 (2020). The global museum: Natural history collections and the future of evolutionary science and

532 public education. *PeerJ*, 8, 1–40. doi:10.7717/peerj.8225

533 Buser, T. J., Boyd, O. F., Cortés, Á., Donatelli, C. M., Kolmann, M. A., Luparell, J. L., ... Summers, A. P.
534 (2020). The natural historian's guide to the CT galaxy: step-by-step instructions for preparing and
535 analyzing computed tomographic (CT) data using cross-platform, open access software. *Integrative*
536 *Organismal Biology*. doi:10.1093/iob/obaa009

537 Capano, J. G. (2020). Reaction forces and rib function during locomotion in snakes. *Integrative and*
538 *Comparative Biology*, 60(1), 215–231. doi:10.1093/icb/icaa033

539 Clement, A. M., Nysjö, J., Strand, R., & Ahlberg, P. E. (2015). Brain–endocast relationship in the
540 Australian lungfish, *Neoceratodus forsteri*, elucidated from tomographic data (Sarcopterygii:
541 Dipnoi). *PLoS One*, 10(10), e0141277.

542 Da Silva, F. O., Fabre, A. C., Savriama, Y., Ollonen, J., Mahlow, K., Herrel, A., ... Di-Poi, N. (2018). The
543 ecological origins of snakes as revealed by skull evolution. *Nature Communications*, 9(1), 1–11.
544 doi:10.1038/s41467-017-02788-3

545 du Plessis, A., Broeckhoven, C., & le Roux, S. G. (2018). Snake fangs: 3D morphological and mechanical
546 analysis by microCT, simulation, and physical compression testing. *GigaScience*, 7(1), 1–8.
547 doi:10.1093/gigascience/gix126

548 Early, C. M., Morhardt, A. C., Cleland, T. P., Milensky, C. M., Kavich, G. M., & James, H. F. (2020).
549 Chemical effects of diceCT staining protocols on fluid-preserved avian specimens. *PloS One*, 15(9),
550 e0238783. doi:10.1371/journal.pone.0238783

551 Fabbri, M., Mongiardino Koch, N., Pritchard, A. C., Hanson, M., Hoffman, E., Bever, G. S., ... Bhullar, B. A.
552 S. (2017). The skull roof tracks the brain during the evolution and development of reptiles including
553 birds. *Nature Ecology and Evolution*, 1(10), 1543–1550. doi:10.1038/s41559-017-0288-2

554 Furat, O., Wang, M., Neumann, M., Petrich, L., Weber, M., Krill, C. E., & Schmidt, V. (2019). Machine
555 learning techniques for the segmentation of tomographic image data of functional materials.
556 *Frontiers in Materials*, 6(June). doi:10.3389/fmats.2019.00145

557 Gans, C. (1969–2010). The Series “Biology of the Reptilia” Volumes 1–22 (1969–2010; 1,366 pages).
558 Edited by Carl Gans, with various individual volumes co-edited by Angus d’A. Bellairs, Thomas S.
559 Parsons, William R. Dawson, Donald W. Tinkle, Kyoko A. Gans, R. Glen Northcutt, Ph.

- 560 Gignac, P. M., & Kley, N. J. (2014). Iodine-enhanced micro-CT imaging: Methodological refinements for
561 the study of the soft-tissue anatomy of post-embryonic vertebrates. *Journal of Experimental*
562 *Zoology Part B: Molecular and Developmental Evolution*, 322(3), 166–176. doi:10.1002/jez.b.22561
- 563 Gignac, P. M., & Kley, N. J. (2018). The utility of DiceCT imaging for high-throughput comparative
564 neuroanatomical studies. *Brain, Behavior and Evolution*, 91(3), 180–190. doi:10.1159/000485476
- 565 Gignac, P. M., Kley, N. J., Clarke, J. A., Colbert, M. W., Morhardt, A. C., Cerio, D., ... Witmer, L. M. (2016).
566 Diffusible iodine-based contrast-enhanced computed tomography (diceCT): An emerging tool for
567 rapid, high-resolution, 3-D imaging of metazoan soft tissues. *Journal of Anatomy*, 228(6), 889–909.
568 doi:10.1111/joa.12449
- 569 Gray, J. A., Sherratt, E., Hutchinson, M. N., & Jones, M. E. H. (2019). Evolution of cranial shape in a
570 continental-scale evolutionary radiation of Australian lizards. *Evolution*, 73(11), 2216–2229.
571 doi:10.1111/evo.13851
- 572 Hedrick, B. P., Heberling, J. M., Meineke, E. K., Turner, K. G., Grassa, C. J., Park, D. S., ... Davis, C. C.
573 (2020). Digitization and the Future of Natural History Collections. *BioScience*, 70(3), 243–251.
574 doi:10.1093/biosci/biz163
- 575 Hedrick, B. P., Yohe, L., Vander Linden, A., Dávalos, L. M., Sears, K., Sadier, A., ... Dumont, E. (2018).
576 Assessing Soft-Tissue Shrinkage Estimates in Museum Specimens Imaged With Diffusible Iodine-
577 Based Contrast-Enhanced Computed Tomography (diceCT). *Microscopy and Microanalysis*, 24(3),
578 284–291. doi:10.1017/S1431927618000399
- 579 Hughes, D. F., Walker, E. M., Gignac, P. M., Martinez, A., Negishi, K., Lieb, C. S., ... & Khan, A. M. (2016).
580 Rescuing perishable neuroanatomical information from a threatened biodiversity hotspot: remote
581 field methods for brain tissue preservation validated by cytoarchitectonic analysis,
582 immunohistochemistry, and x-ray microcomputed tomography. *PLoS One*, 11(5),
583 <http://doi.org/10.1371/journal.pone.0155824>Jackson, T. N. W., Young, B., Underwood, G.,
584 McCarthy, C. J., Kochva, E., Vidal, N., ... Fry, B. G. (2017). Endless forms most beautiful: the
585 evolution of ophidian oral glands, including the venom system, and the use of appropriate
586 terminology for homologous structures. *Zoomorphology*, 136(1), 107–130. doi:10.1007/s00435-
587 016-0332-9
- 588 Lillywhite, H. B. (2014). *How snakes work: Structure, function and behavior of the World's snakes*.

589 Oxford: Oxford University Press.

590 Lister, A. M., Brooks, S. J., Fenberg, P. B., Glover, A. G., James, K. E., Johnson, K. G., ... Young, J. (2011).
591 Natural history collections as sources of long-term datasets. *Trends in Ecology and Evolution*, *26*(4),
592 153–154. doi:10.1016/j.tree.2010.12.009

593 Macrì, S., Savriama, Y., Khan, I., & Di-Poi, N. (2019). Comparative analysis of squamate brains unveils
594 multi-level variation in cerebellar architecture associated with locomotor specialization. *Nature*
595 *Communications*, *10*(1), 1–16. doi:10.1038/s41467-019-13405-w

596 Mataic, D., & Bastani, B. (2006). Intraperitoneal sodium thiosulfate for the treatment of calciphylaxis.
597 *Renal Failure*, *28*(4), 361–363. doi:10.1080/08860220600583781

598 Metscher, B. D. (2009). Micro CT for comparative morphology: Simple staining methods allow high-
599 contrast 3D imaging of diverse non-mineralized animal tissues. *BMC Physiology*, *9*(1).
600 doi:10.1186/1472-6793-9-11

601 Palci, A., Seymour, R. S., Van Nguyen, C., Hutchinson, M. N., Lee, M. S. Y., & Sanders, K. L. (2019). Novel
602 vascular plexus in the head of a sea snake (Elapidae, Hydrophiinae) revealed by high-resolution
603 computed tomography and histology. *Royal Society Open Science*, *6*(9), 0–5.
604 doi:10.1098/rsos.191099

605 Paluh, D. J., Stanley, E. L., & Blackburn, D. C. (2020). Evolution of hyperossification expands skull diversity
606 in frogs. *Proceedings of the National Academy of Sciences of the United States of America*, *117*(15),
607 8554–8562. doi:10.1073/pnas.2000872117

608 Pyron, R. A., Burbrink, F. T., & Wiens, J. J. (2013). A phylogeny and revised classification of Squamata,
609 including 4161 species of lizards and snakes. *BMC Evolutionary Biology*, *13*, 93. doi:10.1186/1471-
610 2148-13-93

611 Schindelin, J., Arganda-Carreras, I., Frise, E., Kaynig, V., Longair, M., Pietzsch, T., ... Cardona, A. (2012).
612 Fiji: An open-source platform for biological-image analysis. *Nature Methods*, *9*(7), 676–682.
613 doi:10.1038/nmeth.2019

614 Schmidbaur, H., Keklikoglou, K., Metscher, B. D., & Faulwetter, S. (2015). Exploring methods to remove
615 iodine and phosphotungstic acid stains from zoological specimens. *Bruker MicroCT User Meeting*
616 *2015*, 116–123.

- 617 Simmons, J. E. (2014). *Fluid preservation: a comprehensive reference*. Rowman & Littlefield.
- 618 Taub, A. M. (1966). Ophidian cephalic glands. *Journal of Morphology*, 118(4), 529–541.
619 doi:10.1002/jmor.1051180406
- 620 Uetz, P. (2020). Species numbers by higher taxa. Retrieved 22 January 2020, from [http://www.reptile-](http://www.reptile-database.org/db-info/SpeciesStat.html)
621 [database.org/db-info/SpeciesStat.html](http://www.reptile-database.org/db-info/SpeciesStat.html)
- 622 Underwood, G. (1967). *Characters useful in the classification of snakes. A contribution to the*
623 *classification of snakes*. London: Trustees of The British Museum (Natural History).
- 624 Williams, F., Bock, A., Doraiswamy, H., Donatelli, C., Hall, K., Summers, A., ... Silva, C. T. (2020). Unwind:
625 Interactive Fish Straightening. *Conference on Human Factors in Computing Systems - Proceedings*,
626 1–13. doi:10.1145/3313831.3376846
- 627 Zuiderveld, K. (1994). *Contrast Limited Adaptive Histogram Equalization*. *Graphics Gems*. Academic
628 Press, Inc. doi:10.1016/b978-0-12-336156-1.50061-6

629 **Table 1.** Collection, staining, and scanning information for 23 museum specimens used in this study. Abbreviations: SVL = snout-vent length;
 630 UMMZ = University of Michigan Museum of Zoology, USA; MUSM = Museo de Historia Natural de la Universidad Nacional Mayor de San Marcos,
 631 Lima, Peru. Asterisks (*) denote historic specimens.

Clade	Taxon	Museum	Specimen	SVL (mm)	Mass (g)	Head diameter (mm)	Number of scans	Days stained	Diffusion rate (mm/day)	Preservation age (years)
Aniliidae	<i>Anilius scytale</i>	UMMZ	248356	495	14.27	7.14	4	4	0.893	2.98
Colubrinae	<i>Chironius fuscus</i>	UMMZ	245047	708	90	10.77	4	5	1.08	3.93
	<i>Psuestes sulphureus</i>	MUSM	37565	1840	1250	30.43	2	12	1.27	2.09
	<i>Lampropeltis abnorma</i>	UMMZ	247095	247	91.4	11.16	4	6	0.93	1.32
	<i>Leptophis ahuetulla</i>	MUSM	37345	565	27.66	9.12	2	5	0.91	1.95
	<i>Tantilla melanocephala</i>	UMMZ	246845	255	7.39	5.51	4	3	0.92	1.95
Dipsadinae	<i>Imantodes cenchoa</i>	UMMZ	246810	876	30.76	7.93	4	5	0.793	2.67
	<i>Helicops angulatus</i>	UMMZ	246805	427	63	12.95	4	5.5	1.18	2.45
	<i>Helicops leopardinus</i>	UMMZ	246808	685	220	18.72	4	9	1.04	2.90
	<i>Leptodeira septentrionaius</i>	UMMZ	247099	654	113.2	14.85	4	6	1.24	1.37
	<i>Nothopsis rugosus</i>	UMMZ	248404	257	6.41	5.45	4	4	0.68	1.33
Elapidae	<i>Oxyrhopus melanogenys</i>	MUSM	37417	230	10.77	6.41	4	6	0.53	3.47
	<i>Xenopholis scalaris</i>	UMMZ	246854	271	7.61	5.94	3	4	0.74	1.81
	<i>Micrurus lemniscatus</i>	MUSM	35905	725	50	9.31	2	4	1.16	2.61
	<i>Micrurus nigrocinctus</i>	UMMZ	247142	717	64.8	12.56	4	6	1.05	1.69
	<i>Micrurus obscurus</i>	UMMZ	246859	261	5.19	6.34	2	5	0.63	2.38
Lamprophiidae	<i>Micrurus surinamensis</i>	MUSM	37353	421	32.47	10.02	4	7	0.72	3.16
	<i>Aparallactus capensis</i> *	UMMZ	61599A	104	8.4	3.26	4	3	0.54	95.62
Viperidae	<i>Atractaspis bibronii</i> *	UMMZ	209986	340	16	6.61	4	4	0.83	25.58
	<i>Bothrops bilineatus</i>	UMMZ	245084	744	85	15.93	4	5	1.59	3.62
	<i>Causus rhombeatus</i> *	UMMZ	65828	410	58	14.55	4	8	0.91	91.62
	<i>Lachesis muta</i>	UMMZ	248369	763	145	21.2	4	11	0.96	3.53

Clade	Taxon	Museum	Specimen	SVL (mm)	Mass (g)	Head diameter (mm)	Number of scans	Days stained	Diffusion rate (mm/day)	Preservation age (years)
	<i>Porthidium nasutum</i>	UMMZ	247139	297	19.1	12.74	4	4	1.59	1.66

633 **Table 2.** Operational costs to set up diceCT scanning facilities and estimate of since diceCT scan after set up. Estimates based on costs at
 634 University of Michigan CT facilities.

Item	Estimate (USD)	Description/model used at the UMMZ
Computer workstation	\$6500-\$10,600	RMC 1040: HP Z4 G4, Intel Core i9, 3.3-4.1GHZ, 16Mb Cache, 8x16GB RAM (128 total), Nvidia Quadro RTX 5000 (16GB RAM). Hewlett-Packard (CA, USA).
Touchscreen monitor	\$1000-\$2000	Optional, for segmentation. Wacom 21" Cintiq 22HD. Wacom (Japan).
Data storage: External hard drives	\$114.99 per drive	5TB external hard drive, Seagate (CA, USA).
Cloud storage	Amazon Cloud: \$59.99/Tb Dropbox: \$99.99/Tb Google Drive: \$99.99/Tb	Prices reflect yearly subscriptions, which vary by vendor.
RAID storage	\$150-\$460	Price varies by vendor. Estimates from Western Digital (CA, USA).
Volume Graphics Studio Max	\$12,000, plus \$2100 per year service contract	Volume Graphics Ltd. (SC, USA)
ORS Dragonfly	Free (academic license)	Segmentation software. ORS (QC, Canada).
Nikon XTH 225ST	\$600,000-800,000	Only if buying a CT scanner. Micro-CT scanner, Nikon (Japan)
Nikon XTH 225 ST service contract	\$22,000 per year	Only if operating a CT scanner. Micro-CT scanner, Nikon (Japan)
Tungsten filament replacements	Option 1 N.1403: \$299.99 for package of 10	Option 1: Ted Pella, Inc (California, USA)
recommended for Nikon XTH 225	Option 2 A054X: \$338 for package of 10	Option 2*: Agar Scientific (Essex, UK)

ST		
Iodine (crystalline)	\$115.60 per 250 grams	99.5%, Lot: Q26E019 Alfa Aesar. Thermo Fisher Scientific (MA, USA).
Potassium iodine	\$299 per 100g	Thermo Fisher Scientific (MA, USA).
Ethanol (EtOH)	\$378.92 per 208.2L drum	Thermo Fisher Scientific (MA, USA).
Packing peanuts	\$29 per 20ft ³ bag	Anti-static, 30% recycled Uline (WI, USA).
Plastic jars	\$00.28-\$1.89 per jar	Clear round wide-mouth plastic jars, Uline (WI, USA).
Soft packing foam	\$61-\$119 based on weight \$16-\$50 based on length and diameter	Soft foam, Uline (WI, USA).
Poly tubing plastic	ordered	Poly tubing plastic dispenser, Uline (WI, USA).
Technician / personnel	\$8000-\$65000 per year	Cost of technician to operate a CT facility depends on employee status (i.e., full time, student, postdoc, part time).
Scanning cost	\$48 per hour	Cost at University of Michigan CT facilities. This cost may vary, and may include packing and set up of the specimen.
Estimated cost of a single diceCT acquisition	\$216 per specimen	Does not include staining, destaining, or any analysis. The average diceCT scan takes 3.5 h, plus an additional 30 minutes before and after for set up and data processing.

635

636 **Figures captions**

637 **Figure 1.** Flow chart of the diceCT process. (a) Illustrated representation of the five steps between
638 selecting a preserved specimen in 75% ethanol and returning it fully de-stained back to the collection.
639 Photos (b), (c), and (d) are the critical components of packing a diceCT snake specimen. (b) Partially heat
640 sealed bag with an encased string to facilitate specimen positioning within the bag, plus a staining
641 specimen card to keep track of staining progress, as described in Section 2.2.3; (c) Stained specimen that
642 has been pulled through the plastic bag using the string (see Section 2.2.3) and fully heat sealed to
643 prevent desiccation during the scan; (d) A packed, stained specimen in the CT scanner. The packing
644 medium is foam packing peanuts (30% recycled polystyrene, Uline, WI, USA) purposefully chosen for
645 their low density, making them not visible in the scan. This mounting position with an elevated, isolated
646 head is ideal as it allows for optimal resolution on cranial scans (see Section 2.2.4). We only used
647 ethanol de-staining in this study, but low concentrations of sodium thiosulfate can be used to accelerate
648 de-staining (see Section 4.1).

649 **Figure 2.** Visual indicators of successful and incomplete iodine staining in preserved snakes. (a) Ventral
650 view of an unstained snake specimen. (b) A specimen immersed in 1.25% Lugol's iodine, which has
651 become partially transparent, the transparent solution indicates incomplete saturation of the specimen
652 and should be replaced with freshly made 1.25% Lugol's iodine. (c) Ventral view of the same specimen
653 shown in (a), fully stained. Note the dark amber colouration and obscuring of body patterns. Specimen
654 in (a) and (b) is a *Helicops leopardinus* (UMMZ 246808) stained for 9 days in 1.25% Lugol's iodine
655 solution. Specimen in (c) is an actively staining *Lampropeltis abnorma* (UMMZ 247095).

656 **Figure 3.** Examples of variation in staining quality among snake head region of interest. (a) Understained
657 specimen that is also distorted by inappropriate foam packing material (2 inch soft foam sheets, Uline,
658 WI, USA). (b) Moderately understained specimen packed in packing peanuts (30% recycled polystyrene,
659 Uline, WI, USA). Note that the left venom gland was dissected before preservation. (c) Understained
660 specimen that is well-contrasted with packing peanuts as packing material. Note the high contrast
661 (oversaturation) of the skeletal system and low contrast of soft tissues. (d) Well stained specimen, with
662 an overstained Harderian gland, packed in packing peanuts. The left Harderian gland was dissected
663 before preservation. Specimen (a) is *Xenopholis scalaris* (UMMZ 246854), (b) *Aparallactus capensis*
664 (UMMZ 61599), (c) *Lachesis muta* (UMMZ 248369), and (d) *Oxyrhopus melanogenys* (MUSM 37417).
665 Specimens were stained in 1.25% Lugol's iodine. L = Lens, Hg = Harderian gland, Vg = Venom Gland.

666 **Figure 4.** (a) Histograms showing mean and range of grayscale values (GV), colours represent total
667 duration in 1.25% Lugol's iodine solution (days), grey boxes indicate select specimens in (b-c); (b) dorsal
668 tomography slices of snake heads; (c) corresponding histograms show distribution of GV for select
669 specimens. Note the variable axes on histograms.

670 **Figure 5.** The relationship between specimen size and duration in 1.25% Lugol's iodine solution: (a)
671 snout-vent length (SVL), (b) mass, (c) head radius. Radii were calculated from the diameter taken at the
672 widest point. 95% confidence intervals shown in grey. Note the ln log scale for mass. Data for SVL and
673 head radius are from 23 species (n = 23 individuals) and data for mass are from 20 species (n = 20
674 individuals) from the snake families Aniliidae, Dipsadinae, Colubrinae, Elapidae, Lamprophiidae and
675 Viperidae.

676 **Figure 6.** Integrating physical dissections with skeletal and diceCT scans can help resolve complex and/or
677 highly variable anatomy. Lateral view of the same preserved specimen: (a) undissected, (b) skinned with
678 venom (Duvernoy's) gland highlighted, (c) skeletal 3D render with the maxillary bone segmented, and
679 (d) diceCT 3D render of the venom gland segmentation and maxillary bone. Eyes are rendered in white
680 for positional reference. Specimen is *Helicops angulatus* (UMMZ 246805).

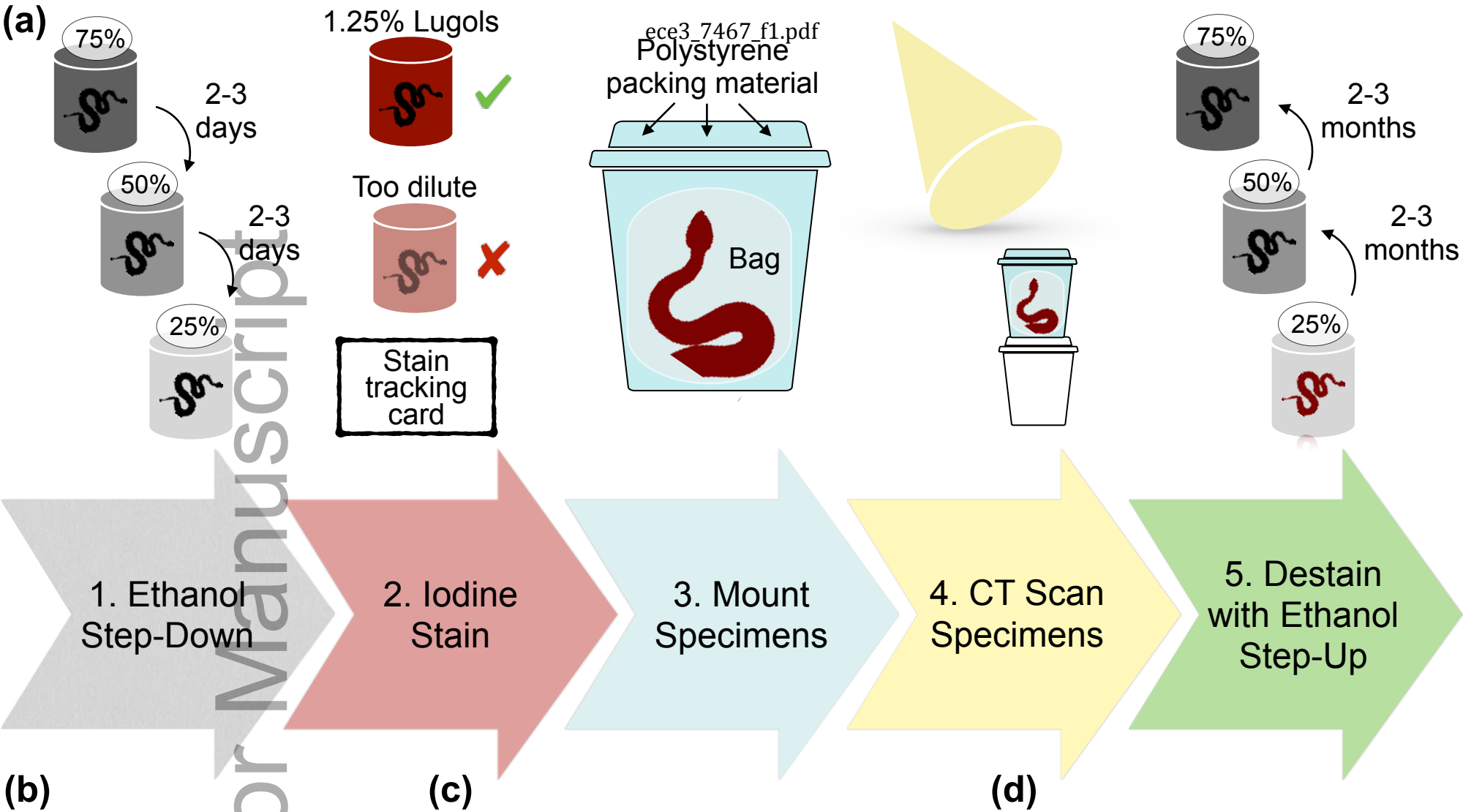
681 **Figure 7.** Combining skeletal and diceCT datasets to explore morphology in venom delivery systems in
682 snakes. Fang morphology and positioning on the maxilla bone differs between (a) Viperidae, tubular
683 front fangs (solenoglyphous), (b) Elapidae, hollow front fangs (proteroglyphous), and (c) Colubridae,
684 grooved or unmodified rear fangs (opisthoglyphous). DiceCT can be used to visualize and quantify soft-
685 tissue anatomy (venom and accessory glands, duct connections, muscle) with fang traits to build an
686 integrative comparison of venom systems across taxa. ag = accessory gland, d = duct, f = fang, m =
687 muscle. vg = venom gland.

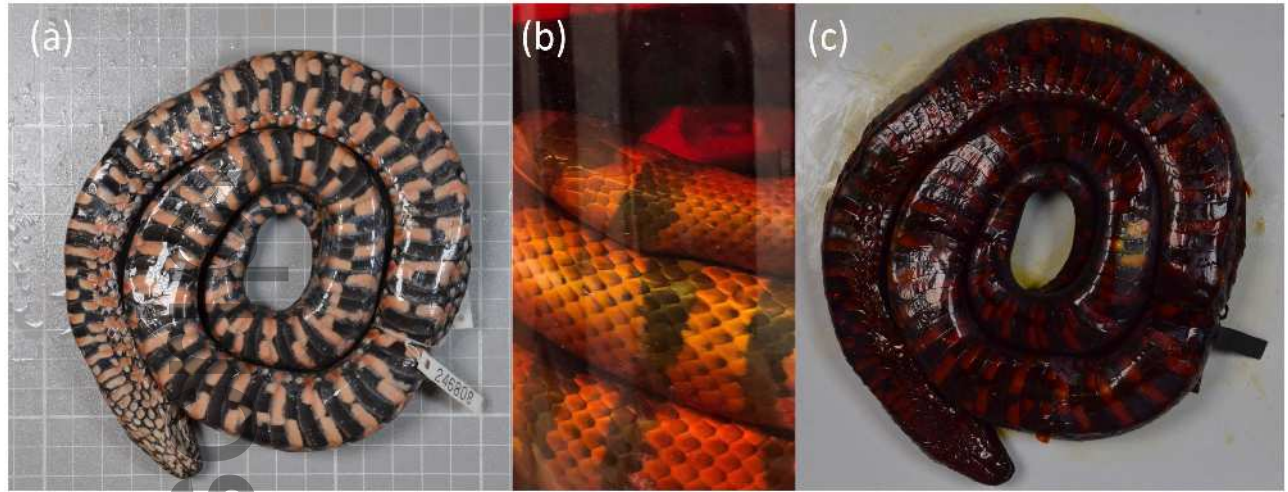
688 **Figure 8.** DiceCT data allows for morphological comparisons *in situ*, which makes it an important
689 technique for studies of trait evolution, especially systems that evolve in unison such as neural and
690 sensory anatomy. (a) Dorso-lateral view of a whole brain segmentation of *Imantodes cenchoa* (UMMZ-
691 346810). (b) Dorsal view of a tomography slice with 3D segmentations of the visual system. (c) Dorsal
692 view of a tomography slice with 3D segmentations of the vomeronasal system. Image credit: Consuelo
693 Alarcón Rodríguez.

694 **Figure 9.** Natural history bycatch: two full body scans of the same specimen (UMMZ 247099) show a
695 recent prey item and gravidity in a female *Leptodeira septentrionalis*. (a) Lateral view of combined dice

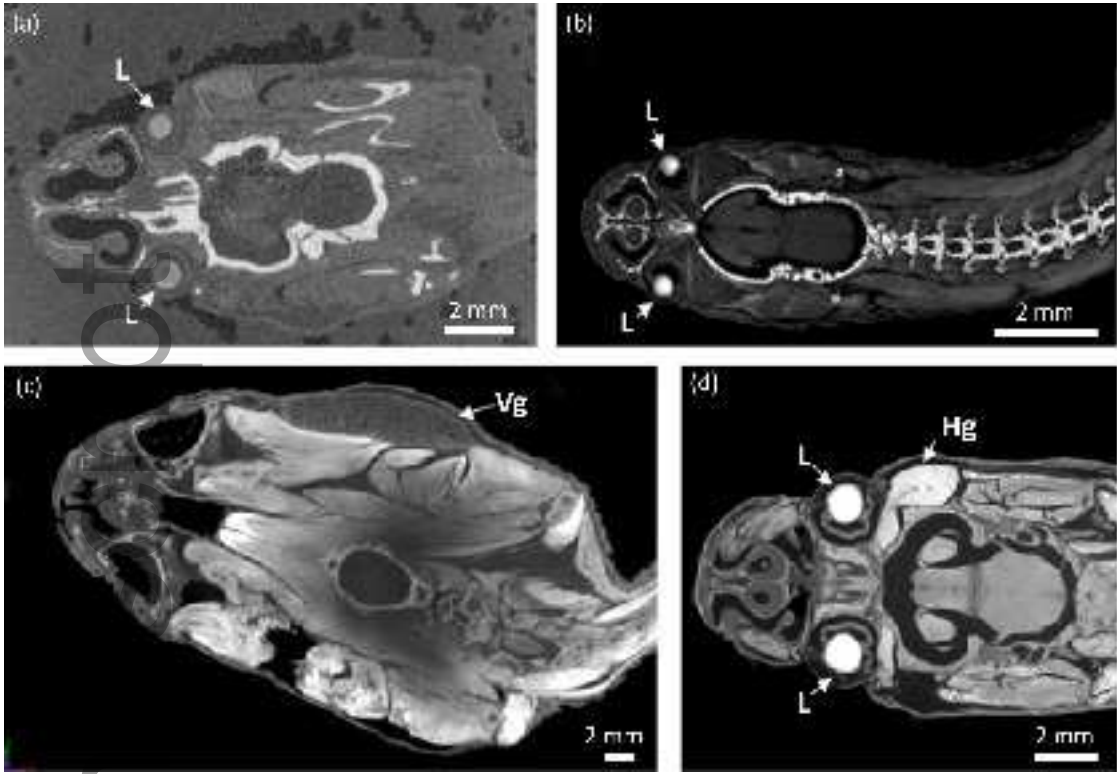
696 and skeletal CT scans. (b) Ventral view of snake skeletal scan with prey segmentation in green. Anuran
697 prey was identified by presence of the urostyle (u). (c) Ventral view of snake diceCT scan with eggs
698 segmentation in orange.

Author Manuscript



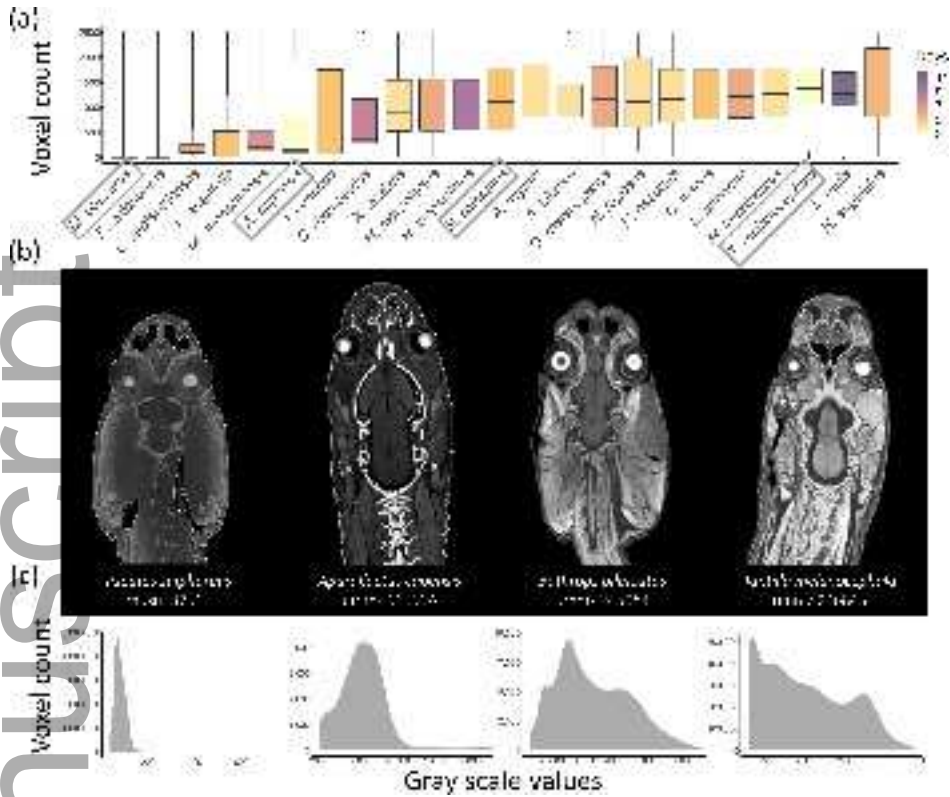


ece3_7467_f2.tif

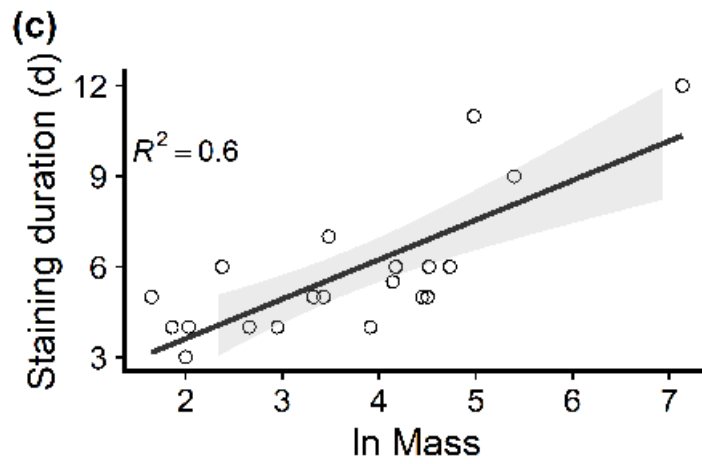
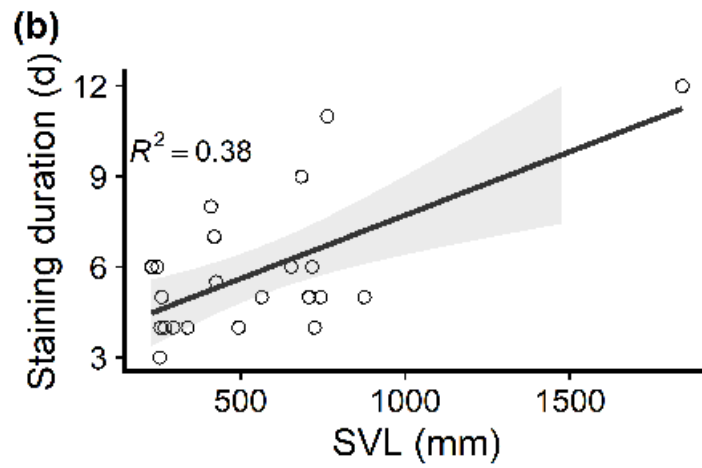
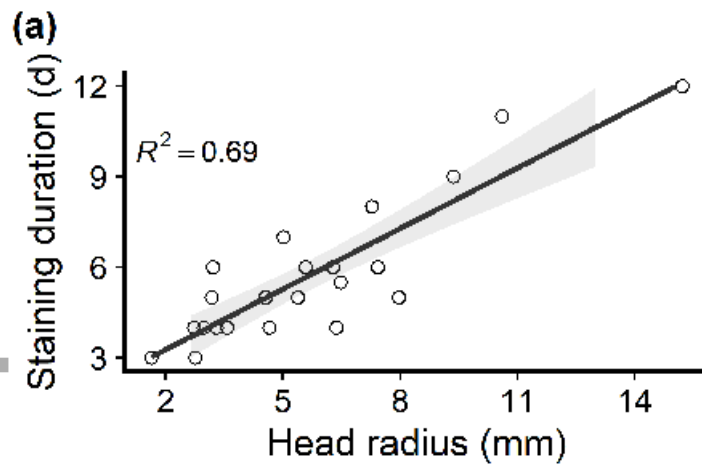


ece3_7467_f3.tif

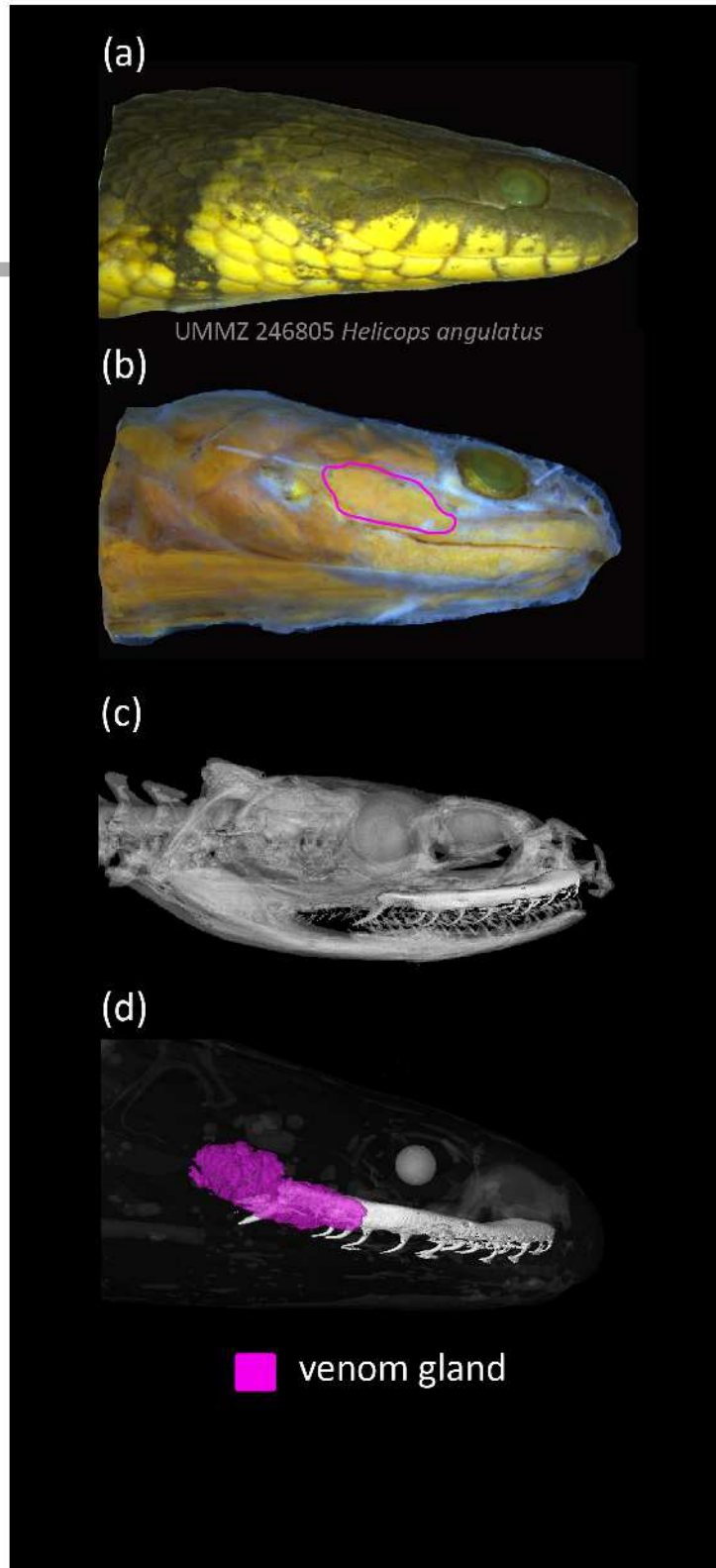
Author Mar

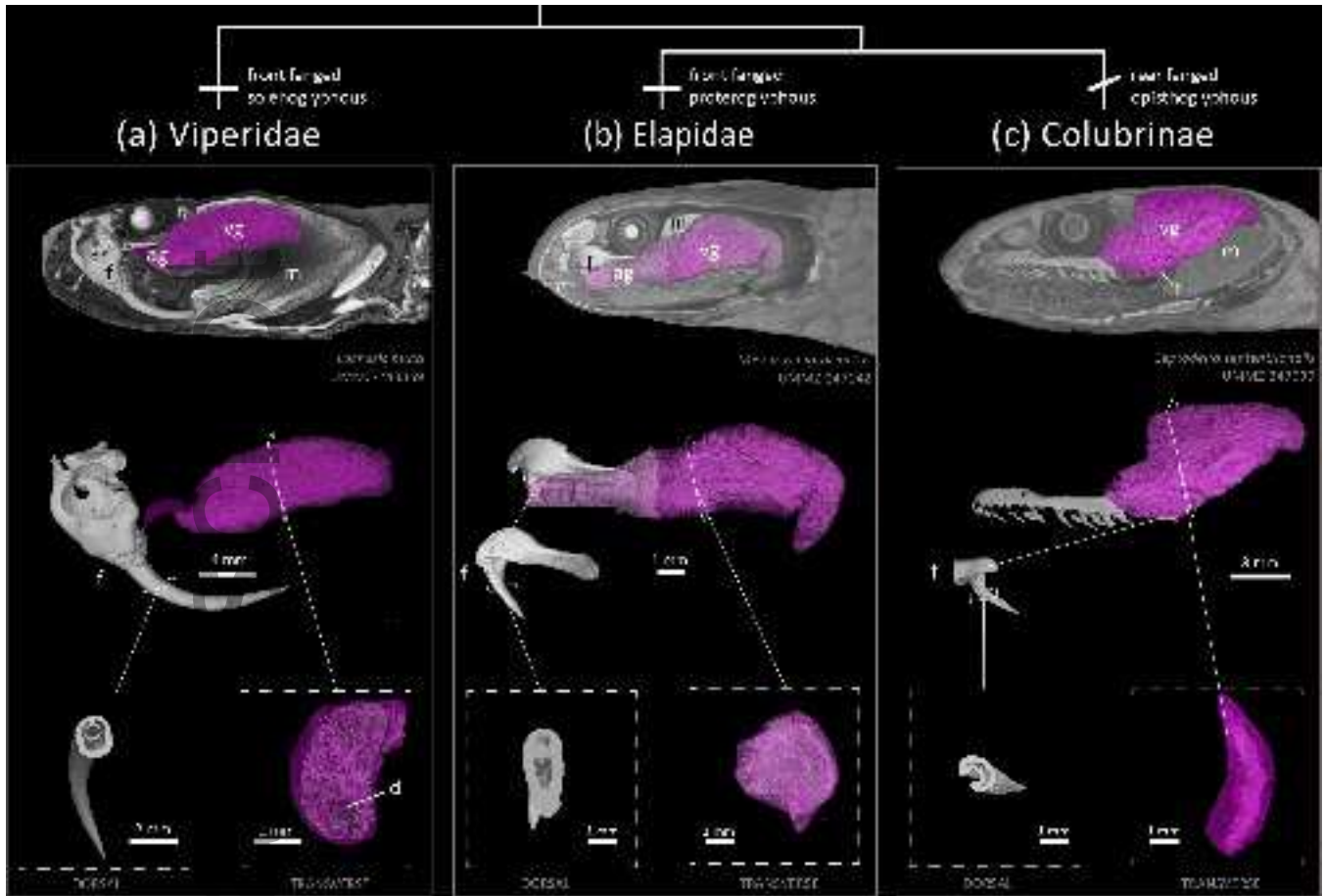


ece3_7467_f4.tif



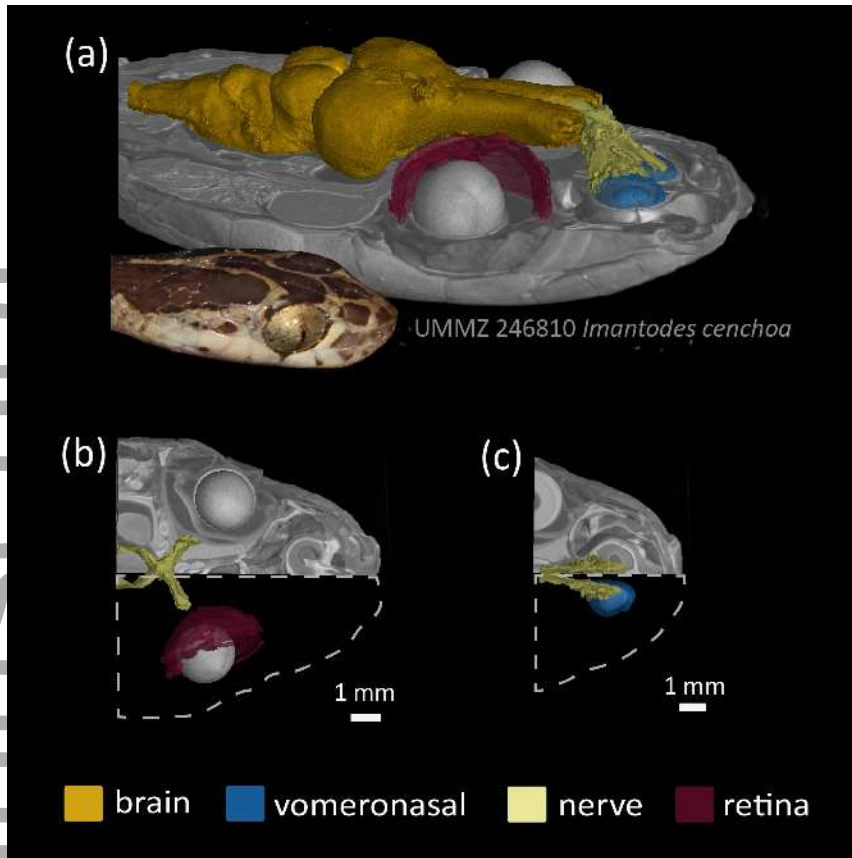
ece3_7467_f5.tif



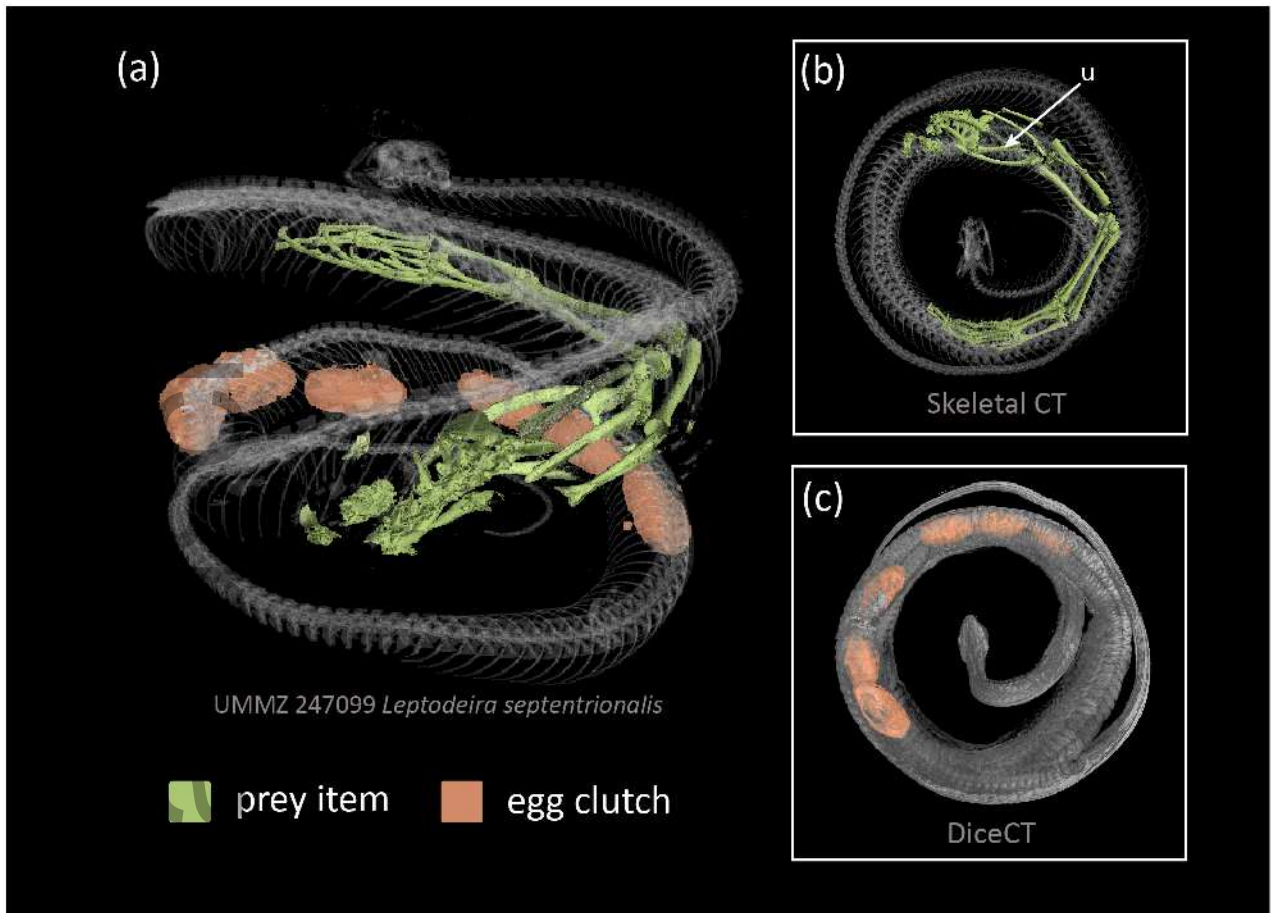


ece3_7467_f7.png

Author Manuscript



ece3_7467_f8.tif



Author N

ece3_7467_f9.tif